

Galaxy and Mass Assembly (GAMA): galaxy radial alignments in GAMA groups

Michael D. Schneider^{1,2*}, Shaun Cole³, Carlos S. Frenk³, Lee Kelvin^{4,5},
Rachel Mandelbaum^{6,7}, Peder Norberg³, Joss Bland-Hawthorn⁸, Sarah Brough⁹,
Simon Driver^{4,5}, Andrew Hopkins⁹, Jochen Liske¹⁰, Jon Loveday¹¹, Aaron Robotham^{4,5}

¹*Department of Physics, University of California, One Shields Avenue, Davis, CA 95616, USA.*

²*Lawrence Livermore National Laboratory, P.O. Box 808 L-210, Livermore, CA 94551-0808, USA.*

³*Institute for Computational Cosmology, Department of Physics, Durham University, South Road, Durham, DH1 3LE, UK.*

⁴*School of Physics and Astronomy, University of St Andrews, North Haugh, St. Andrews, Fife KY16 9SS.*

⁵*International Centre for Radio Astronomy Research, 7 Fairway, The University of Western Australia, Crawley, Perth, WA 6009, Australia.*

⁶*Princeton University Observatory, Peyton Hall, Princeton, NJ 08544 USA.*

⁷*Department of Physics, Carnegie Mellon University, Pittsburgh, PA 15213, USA.*

⁸*Sydney Institute for Astronomy, University of Sydney, NSW 2006, Australia.*

⁹*Australian Astronomical Observatory, PO Box 296, Epping, NSW 1710, Australia.*

¹⁰*European Southern Observatory, Karl-Schwarzschild-Str. 2, 85748 Garching bei M unchen, Germany.*

¹¹*Astronomy Centre, University of Sussex, Falmer, Brighton, BN1 9QH, UK.*

LLNL-JRNL-544911

ABSTRACT

We constrain the distributions of projected radial alignment angles of satellite galaxy shapes within the Galaxy And Mass Assembly survey group catalogue. We identify the galaxy groups using spectroscopic redshifts and measure galaxy projected ellipticities from Sloan Digital Sky Survey imaging. With a sample of 3850 groups with 13655 satellite galaxies with high quality shape measurements, we find a less than $2\text{-}\sigma$ signal of radial alignments in the mean projected ellipticity components and the projected position angle when using galaxy shape estimates optimized for weak lensing measurements. Our radial alignment measurement increases to greater than $3\text{-}\sigma$ significance relative to the expectation for no alignments if we use 2-D Sérsic model fits to define galaxy orientations. Our weak measurement of radial alignments is in conflict with predictions from dark matter N -body simulations, which we interpret as evidence for large mis-alignments of baryons and dark matter in group and cluster satellites. Within our uncertainties, that are dominated by our small sample size, we find only weak and marginally significant trends of the radial alignment angle distributions on projected distance from the group centre, host halo mass, and redshift that could be consistent with a tidal torquing mechanism for radial alignments. Using our lensing optimized shape estimators, we estimate that intrinsic alignments of galaxy group members may contribute a systematic error to the mean differential projected surface mass density of groups inferred from weak lensing observations by $-1 \pm 20\%$ at scales around $300 h^{-1}\text{kpc}$ from the group centre assuming a photometric redshift r.m.s. error of 10%, and given our group sample with median redshift of 0.17 and median virial masses $\sim 10^{13} h^{-1}M_{\odot}$.

Key words: galaxies: clusters: general – galaxies: formation – galaxies: statistics.

1 INTRODUCTION

The hierarchical model for cosmological structure formation posits that groups and clusters of galaxies form by the ac-

cretion of smaller groups and individual galaxies. In this scenario, as galaxies are accreted into a group they would be tidally torqued so that their major axes would be aligned with the centre of the gravitational potential well. The efficiency of torquing within a cluster should depend on the gradient of the potential well and the eccentricity of the ac-

* E-mail: schneider@ucdavis.edu

creted galaxy's orbit (Pereira et al. 2008) as well as the rotational support (or lack thereof) of the infalling galaxy (Wesson 1984). This simple picture then predicts that satellite galaxies should be more radially aligned in more concentrated (i.e. typically lower mass) groups and that the degree of alignment should have an inverse relation to the angular speed of the galaxy thereby imparting a dependence on the distance from the potential centre (Kuhlen et al. 2007; Pereira et al. 2008; Pereira & Bryan 2010).

This tidal torquing model for the radial alignments of satellite galaxies could be complicated by effects such as the tidal stripping of infalling satellites or the misalignments of stars and dark matter due to complex accretion and merger histories. Alternatively, if the time-scales for tidal torquing in a group or cluster are comparable to the age of the Universe, then any global alignments of cluster galaxies may instead serve as a probe of the anisotropic accretion history from filaments around the cluster (Djorgovski 1983; Wesson 1984; Adami et al. 2009; Song & Lee 2012), in which case no radial alignments should be detected. Observations seeking to measure radial alignments are further confounded by the difficulty in measuring unbiased galaxy shapes and orientations, the projection of unknown 3D galaxy morphologies into the plane of the sky, and the unknown location of the group or cluster potential centre.

Using photographic plates covering three nearby clusters, Hawley & Peebles (1975) rejected the null hypothesis of uniform projected radial alignment angles at roughly 98 percent significance in the Coma cluster (only). Djorgovski (1983) later found significant radial alignments in the Coma cluster, with faint and red galaxies near the cluster centre showing the strongest alignments. With the large galaxy samples in the more recent redshift and cluster surveys, several groups have claimed both strong detections of radial alignments (Pereira & Kuhn 2005; Agustsson & Brainerd 2006; Faltenbacher et al. 2007) and null detections (Bernstein & Norberg 2002; Siverd et al. 2009; Hao et al. 2011; Hung & Ebeling 2012; Blazek et al. 2012). See Hao et al. (2011) their table 1, for a comparison of measurements in the Two-degree-Field Galaxy Redshift Survey (2dFGRS) and Sloan Digital Sky Survey (SDSS). Siverd et al. (2009) and Hao et al. (2011) showed that measurements of satellite galaxy orientations using SDSS isophotes may be subject to numerous systematics that could potentially resolve the discrepant claims of detection and null signals in the literature. We will address this issue further in Section A.

The 3D radial alignments of dark matter sub-haloes within cluster-sized parent haloes have been measured in N -body simulations (Kuhlen et al. 2007; Pereira et al. 2008; Knebe et al. 2008a), showing much stronger radial alignments than in any observations independent of parent or sub-halo mass. Kuhlen et al. (2007) and Knebe et al. (2008b) showed that using only the inner 10–20% of the particles in a dark matter sub-halo, rather than all bound sub-halo particles, introduces significant scatter in the distribution of radial alignment angles that is more consistent with previous observations. Using N -body simulations with gas and star formation physics included, Knebe et al. (2010) concluded that gas physics does not measurably affect the radial alignment angles of satellite galaxies relative to the orientations inferred from studying the parent dark matter sub-haloes alone. Pereira & Bryan (2010) performed isolated N -body

simulations of a satellite falling into a cluster potential to study the tidal torquing effect as a function of orbital phase and find a strong dependence of the radial alignment angle on the orbital angular velocity, which was a conclusion also found by Kuhlen et al. (2007) and Knebe et al. (2010) in their simulations embedded in a cosmological environment. Together, these simulation studies have established the tidal torquing mechanism as the dominant effect on satellite radial alignments and as a key prediction for structure formation in cold dark matter theories.

The anisotropic accretion of satellites on to groups and clusters also tends to align satellites with the parent cluster major axis (e.g. Dekel 1985; Plionis et al. 2003). The measurement of this effect is beyond the scope of this paper, but we note that such alignments could dilute the radial alignment measurement when approximating triaxial groups with a spherical geometry.

Models for the alignments of group and cluster members are also important for predicting and mitigating the intrinsic alignment contamination in weak lensing studies (e.g. Hirata et al. 2004; Mandelbaum et al. 2006a; Hui & Zhang 2008; Schneider & Bridle 2010; Kirk et al. 2010). Bernstein & Norberg (2002) explicitly constrained the lensing contamination from their measured radial alignments, but we will focus more on constraining models for the radial alignment angle distributions that could be later propagated into predictions for intrinsic alignment contamination in lensing measurements.

In this paper we constrain the distributions of projected radial alignments of galaxy group satellites in the Galaxy and Mass Assembly (GAMA) survey¹ (Driver et al. 2009; Baldry et al. 2010; Robotham et al. 2010; Hill et al. 2011; Driver et al. 2011). All group members in the GAMA catalogue are spectroscopically confirmed and the group properties have been calibrated by comparison with mocks built from N -body simulations (Robotham et al. 2011). As in some other recent studies, we measure satellite galaxy orientations from SDSS imaging. We use two estimates of the galaxy shapes, the 2D galaxy model fits to SDSS r -band imaging data which account for the effects of point spread function (PSF) convolution using the SIGMA pipeline as described in Kelvin et al. (2012) and a galaxy shape estimator optimized for weak lensing that is more sensitive to the shapes of galaxies at smaller radii (Hirata & Seljak 2003; Mandelbaum et al. 2005).

This paper is organized as follows. We describe the relevant features of the GAMA galaxy group catalogue in Section 2.1 and the galaxy shape estimators in Section 2.2. We present and compare our measures of galaxy radial alignments in groups in Section 3.1. We use mock group catalogues with model radial alignments as described in Section 3.2 to assess the significance of our measurements. We then show our measurements in Section 4 and discuss their implications in Section 5. To aid the comparison with previous analyses based on SDSS imaging, we compare our shape estimators with the isophote measurements in the SDSS Catalog Archive Server² (CAS, Thakar et al. 2008) in Appendix A.

¹ <http://www.gama-survey.org/>

² <http://cas.sdss.org/>

2 DATA DESCRIPTION

In this section we describe the data sets and analysis pipelines we have combined to perform our analysis.

2.1 Group catalogue

We use the GAMA-I galaxy group catalogue (G³Cv1) as described in Robotham et al. (2011) to define the group memberships and global group properties. The G³Cv1 catalogue contains 4263 groups with three or more members identified within $\sim 142 \text{ deg}^2$ with a spectroscopic depth limit of $r_{AB} = 19.4$ (with 98% completeness Driver et al. 2011). We define group redshifts to be the median redshift of all group members, which span 0.017 to 0.46 with a mean redshift for the group catalogue of 0.18. By comparing with mock group catalogues built with N -body simulations, Robotham et al. (2011) assigned dark matter halo masses to each group. We assign halo masses to match the observed group velocity dispersions, which can lead to some spuriously large or small halo mass estimates. However, 95 percent of the groups with three or more members have halo masses in the range 4.4×10^{10} to $8.6 \times 10^{14} h^{-1} M_{\odot}$, where h is reduced Hubble constant. In addition to the robust determination of group membership, our study is sensitive to the determination of the group centre about which the satellite galaxy alignments are measured. Throughout, we use the “iterative group centre” that Robotham et al. (2011) showed to be more accurate than assuming the Brightest Cluster Galaxy (BCG) is at the group centre (if the BCG can be accurately determined).

The observed angular separations between satellite galaxies and the group centres are converted to physical co-moving distances using the median group redshift to calculate the angular diameter distance to the group assuming a cosmology of $\Omega_m = 0.25$ and $\Omega_{\Lambda} = 0.75$ (which is used consistently throughout the GAMA group catalogue construction).

2.2 Galaxy shape measurements

For our primary method of galaxy shape determination, we use the shape measurements from the REGLENS pipeline applied to SDSS imaging as described in Hirata & Seljak (2003) and Mandelbaum et al. (2005). The REGLENS shape estimates use a re-Gaussianization (Hirata & Seljak 2003) algorithm to correct for the effects of the PSF on the observed galaxy shapes. Briefly, REGLENS finds best-fit (in the least-squares sense) 2-D Gaussians to both the PSF and the observed galaxy image. The galaxy ellipticity is defined by a 2-D covariance matrix derived from the difference of the best-fit image and PSF covariances. A ‘resolution’ factor is then defined by the fractional deviation of the traces of the PSF and the re-Gaussianized image covariances. First order corrections to both the resolution factor and ellipticity estimate are applied to account for deviations of the PSF and image from a Gaussian profile. Because the Gaussian profile is a steeply falling function of galactic radius, REGLENS tends to be most sensitive to the shapes of galaxies at much smaller radii than typical model fits, which we describe next. This is an advantage for the purpose of unbiased shear estimation in weak lensing studies, but may not be the optimal choice for probing the physical mechanisms behind

intrinsic galaxy alignments. The REGLENS pipeline also includes quality cuts based on the resolution of the galaxy images, galactic extinction, and seeing quality that reduce our group catalogue to 3862 groups with 13956 galaxies from 4263 groups with 21132 galaxies before the shape quality cuts are applied. The size cuts for the REGLENS pipeline are described in section 2.2.1 of Mandelbaum et al. (2005). The REGLENS galaxies must have a resolution factor of $> 1/3$. In addition, we select only those satellite galaxies with ellipticity magnitudes, as measured by the REGLENS pipeline, greater than 0.05. This minimum ellipticity magnitude cut further reduces our sample to 3850 groups and 13,655 galaxies.

For comparison with previous studies of radial alignments and to test the robustness of our results with respect to the choice of galaxy shape estimator, we also define galaxy shapes based on a 2-D Sérsic model fit to r -band SDSS imaging output by the SIGMA pipeline as part of the GAMA survey and described in Kelvin et al. (2012). The SIGMA outputs can be found in the GAMA Sérsic Photometry catalogue, version 7 (SersicCatv07). The SIGMA outputs we use here are the effective half-light radius along the semi-major axis r_e , galaxy ellipticity $e_{\text{SIGMA}} \equiv 1 - b/r_e$ with b the semiminor axis length, the position angle θ (relative to a fixed coordinate system) and Sérsic index (used in Section 4 as a proxy for morphology). Kelvin et al. (2012) fit a PSF-convolved 2-D Sérsic model as well as neighbouring stars and galaxies so that the SIGMA outputs should not be strongly contaminated by the rounding effect of the PSF or blending with nearby objects. The PSF model is defined by centroid and width parameters and is fit earlier in the SIGMA pipeline before fitting the galaxy profiles. For consistency with REGLENS and common weak lensing analyses, we redefine the ellipticity magnitude in the SIGMA catalogue as,

$$e \equiv \frac{a^2 - b^2}{a^2 + b^2}, \quad (1)$$

where $a \equiv r_e$ and $b \equiv r_e(1 - e_{\text{SIGMA}})$. We further define ellipticity measurement errors by formally propagating the reported SIGMA errors in r_e and e_{SIGMA} . We discarded approximately 2% of the galaxies that passed the REGLENS quality cuts at this stage because the formally propagated ellipticity errors were outside the interval $[0, 1]$. In contrast to previous radial alignment measurements using SDSS isophotes, the ellipticities obtained from the SIGMA pipeline have stellar PSF models incorporated in the fits to the galaxy profiles. In Appendix A we compare the SIGMA and independent GAMA isophote properties with the isophotes available in the SDSS CAS catalogue, which lacks the PSF correction present in SIGMA.

The REGLENS shapes are weighted to measure the inner shapes of galaxies while the SIGMA shapes also utilize information on the shape in the far outskirts of a galaxy image. The SIGMA shapes are potentially more sensitive to bias from sky background subtraction uncertainties and nearby neighbours in the imaging (Siverd et al. 2009), although the careful pipeline in Kelvin et al. (2012) attempts to mitigate these issues. This also causes the SIGMA shapes to be more sensitive to astrophysical mechanisms that affect the outskirts of galaxy light distributions, which may include the tidal torquing mechanism we investigate here.

3 METHODS

3.1 Measures of radial alignments

We consider two common statistics for measuring the projected radial alignments of galaxies in groups and clusters.

3.1.1 Position angle

The galaxy position angle, ϕ , is defined as the angle between the projected galaxy shape major axis (however this is defined) and the projected radius vector of the galaxy position from the group centre, as shown in the left-hand panel of Fig. 1. When the position angle equals zero, the galaxy is perfectly aligned with the projected group radius vector. Because the galaxy shape is symmetric under 180° rotations in the plane of the sky, the position angle is defined in the interval $(-\pi/2, \pi/2]$. In the right-hand panel of Fig. 1 we show some model probability distributions for ϕ , with periodicity imposed. The short-dashed green line is a fit to the distribution found in the N -body simulations of Pereira et al. (2008) while the solid red line is the best fit to our data as described in Section 4 below. The long-dashed blue line shows the uniform distribution.

3.1.2 Ellipticity components

Given a measurement of the projected ellipticity components of a galaxy in a global coordinate system, the x and y components of the projected ellipticity can be conveniently represented as the real and imaginary parts of a complex number,

$$\mathbf{e} = |\mathbf{e}| e^{2i\phi_e}. \quad (2)$$

For considering orientations within a group or cluster it is convenient to further define the rotated ellipticity components,

$$\mathbf{e}_+ + i\mathbf{e}_\times = -\mathbf{e} e^{-2i\phi}, \quad (3)$$

where ϕ is the azimuthal angle of the galaxy projected position with respect to the centre of the group, i.e. the position angle as defined in Section 3.1.1. A positive \mathbf{e}_+ component indicates a tangential alignment of the galaxy with respect to the group centre while a negative \mathbf{e}_+ indicates a radial alignment. The \mathbf{e}_\times ellipticity component indicates satellite galaxy orientations at $\pm 45^\circ$ to the galaxy position vector. The \mathbf{e}_\times component is expected to have a zero mean for every group in the absence of a coherent ‘‘curl’’ component in the galaxy alignments, which is not motivated by any physical model that we know of. Therefore, a group with radially aligned galaxies would have negative mean \mathbf{e}_+ and zero mean \mathbf{e}_\times components.

The observed ellipticity components are a combination of the intrinsic projected ellipticities of the galaxies and shears induced by gravitational lensing. Because the foreground lensing masses are unlikely to have symmetries matching those of the background galaxy groups, and because we only consider averages of the group satellite ellipticities, we do not expect lensing distortions to bias our results.

3.1.3 Weighted estimators for radial alignment measures

To down-weight galaxies with noisy shape estimates and to better apply our results to predictions of weak lensing intrinsic alignment contamination, we compute the mean ellipticity components using an inverse noise weighting per galaxy common for lensing measurements,

$$w_e \equiv (e_{\text{RMS}}^2 + \sigma_e^2)^{-1}, \quad (4)$$

where σ_e is the measurement error per ellipticity component and e_{RMS} is the r.m.s. ellipticity magnitude of our sample. Both the REGLENS and SIGMA samples have $e_{\text{RMS}} \approx 0.37$. Because we are using bright galaxies, e_{RMS} is typically much larger than the ellipticity measurement errors yielding nearly equal weighting for most galaxies when computing the mean ellipticity components.

While the position angle is not a statistic used for lensing measurements, we adopt identical weights for computing the mean position angles of our samples in order to down-weight galaxies with large position angle uncertainties. We derive position angle measurement uncertainties by formally propagating the ellipticity component measurement uncertainties. We therefore find a strong correlation between position angle error and ellipticity magnitude, with more round galaxies having larger position angle uncertainties. Our weights then favour more elliptical galaxies when computing the mean position angles.

3.1.4 Comparison of galaxy shape estimators

In Fig. 2 we compare the \mathbf{e}_+ components for all satellite galaxies in our group catalogue that passed the REGLENS galaxy shape quality cuts. The dashed line in Fig. 2 has a slope of one and passes through the origin. There is overall good agreement between the two shape estimators with larger scatter for smaller ellipticity magnitudes (i.e. rounder images) as expected.

We compare the position angle for our two shape estimators in Fig. 3. The scatter in the position angle derived from our two shape estimators is comparable to our estimate in the formal error on the mean position angle of 6° , indicating that global statistical measures based on the two shape estimators should have a high degree of consistency. By selecting only those galaxies with ellipticity magnitudes greater than ~ 0.4 we find we can reduce the scatter between the shape estimators seen in Fig. 3, indicating some of the scatter is due to different handling of rounder galaxies where the position angle becomes poorly defined.

As previously pointed out by Siverd et al. (2009), large isophote ellipticity does not necessarily imply high shape measurement accuracy in the presence of systematic errors such as isophotal twisting or confusion with nearby objects. Because SIGMA orientations are more sensitive to galaxy shapes at larger radii than REGLENS, isophotal twisting may contribute to the scatter in Fig. 3. That is, physical differences in the shapes of galaxies at different galactic radii are expected to produce scatter in the position angles derived from different shape estimators, even in the absence of other sources of uncertainty.

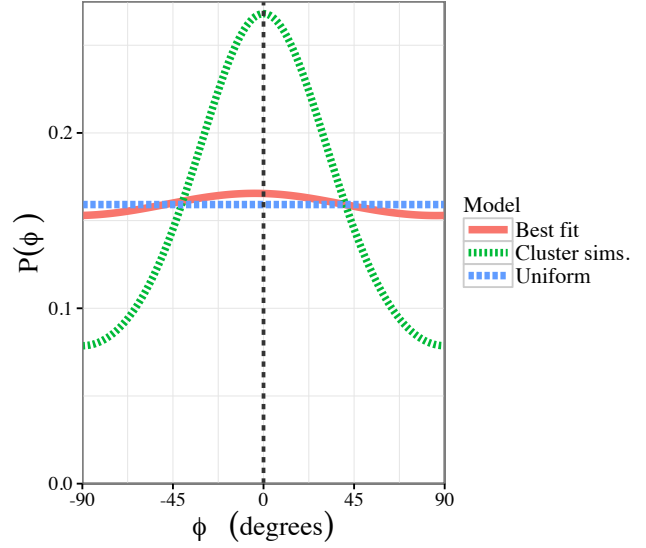
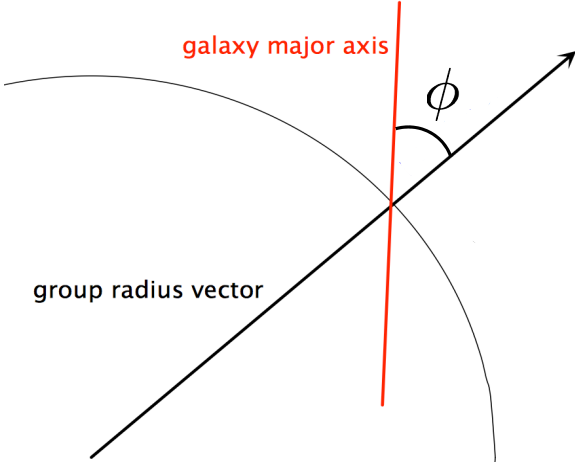


Figure 1. Left: definition of the *position angle* (ϕ) of a satellite galaxy. Due to the rotational symmetry in the plane of the sky, the position angle is defined on $[-\pi/2, \pi/2]$. Right: the probability distribution of the position angle based on the von Mises distribution (see the text) for the best fit to the GAMA groups with three or more members (red solid line), a prediction from isolated cluster N -body simulations (short dashed green line), and the uniform distribution (long dashed blue line).

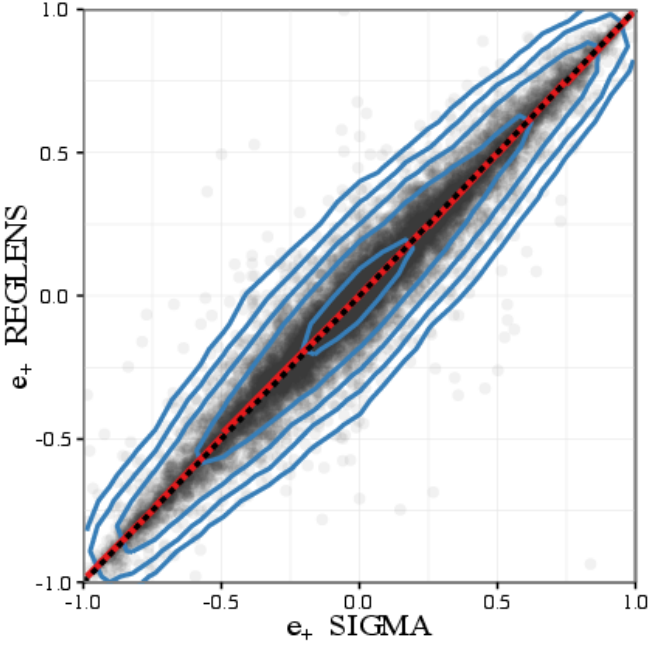


Figure 2. Comparison of the ellipticity component measuring radial alignment derived from two different galaxy shape estimators for all groups with three or more members. The logarithmically spaced blue con tours trace the density of the plotted points. The dashed black line shows a slope of one going through the origin.

3.2 Mock catalogues

To assess the significance of our measured radial alignment statistics we measure identical statistics in an ensemble of mock galaxy group catalogues described in detail in Robotham et al. (2011). Robotham et al. (2011) con-

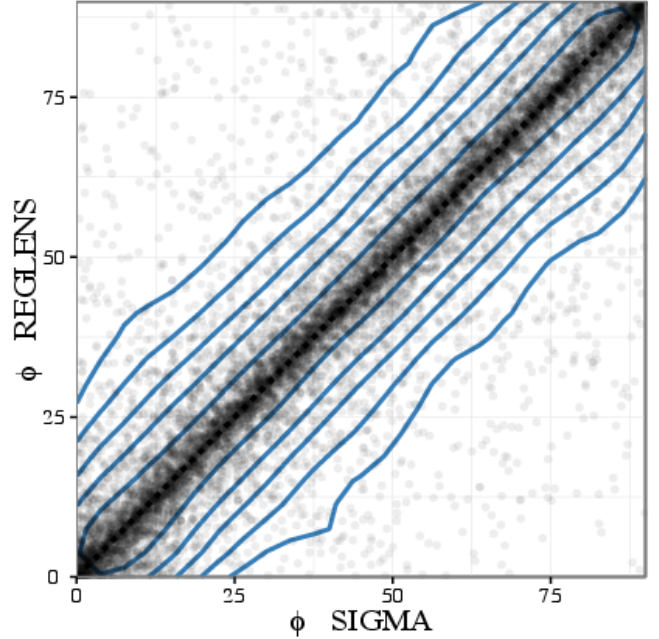


Figure 3. Comparison of the satellite galaxy position angle with respect to the group radius vector derived from two different galaxy shape estimators for all groups with three or more members. The logarithmically spaced blue con tours show the density of points for all satellite galaxies with REGLENS $|e| > 0.05$. The dashed black line shows a slope of one going through the origin.

structed nine mock catalogues based on populating galaxies in the Millennium N -body dark matter simulation³, matching many properties of the galaxies and groups to the data to

³ <http://www.mpa-garching.mpg.de/galform/millennium/>

infer the unobservable properties of the dark matter haloes surrounding each group. For each of the 9 mock catalogues, we make 25 different mock realizations of the satellite galaxy alignments by assigning each satellite galaxy in the mock a projected alignment angle drawn from a parametrized distribution. The distribution of mean radial alignment measures derived from the 9×25 mock realizations gives us a theoretical probability for assessing the significance of the observed mean radial alignment statistics.

While it would be possible in principle to assign satellite galaxy orientations according to the 3D shapes and orientations of the satellite dark matter haloes in the mocks, we take a simpler approach in this paper that is more directly related to the observable projected galaxy shapes and assign the projected satellite position angles, ϕ , by drawing from a von Mises distribution (Lund & Agostinelli 2009),

$$p(2\phi|\mu, \kappa) \equiv \frac{e^{\kappa \cos(2\phi - \mu)}}{2\pi I_0(\kappa)}, \quad (5)$$

with the same parameters $\mu \in [-\pi, \pi]$ and $\kappa > 0$ for every mock satellite, where I_0 is the zeroth order modified Bessel function of the first kind. Unlike the commonly used Gaussian distribution, the von Mises distribution (defined here with argument 2ϕ) has finite support on $[-\pi, \pi]$, limiting $-\pi/2 \leq \phi \leq \pi/2$. This is important when the variance of ϕ is large. In the limit of small standard deviation σ , the parameter $\kappa \sim 1/\sigma^2$. When $\kappa = 0$ the von Mises distribution becomes the uniform distribution over the defined interval of support. So, any constraint on $\kappa > 0$ constitutes a detection of non-uniformity in the position angle distribution. The mock satellite ellipticity magnitudes are drawn from a fit to the distribution of observed ellipticity magnitudes for a given multiplicity cut and, in some cases, binning in group mass and radius.

Given the 2-D positions of each galaxy in the GAMA mocks and the group membership, we compute the angle of the radius vector to each group satellite galaxy and then add the angle ϕ drawn from equation (5). Because this algorithm is sensitive to the group centre definition, we draw systematic group centre offsets from a distribution that fits the histograms for the ‘‘Iter’’ group centres in fig. 3 of Robotham et al. (2011).

4 RESULTS

The ellipticity component measuring radial or tangential alignment is shown in Fig. 4 versus projected physical separation from the group centre for all groups with 3 or more group members. We used the ‘‘iterative centre’’ and the median group redshifts from the GAMA group catalogue to calculate the projected physical separation of the satellites from the group centres. The dashed red lines show the median and first and third quartiles of the e_+ values in bins in the projected radius. If the satellites in our catalogue were strongly radially aligned, the points and lines in Fig. 4 would be skewed below zero. Because the points and lines in Fig. 4 are approximately symmetric and broadly distributed about zero, we can infer that any projected radial alignment signal in our group catalogue is sufficiently weak that we have limited statistical power to measure it.

For satellite orientations uniformly distributed in the

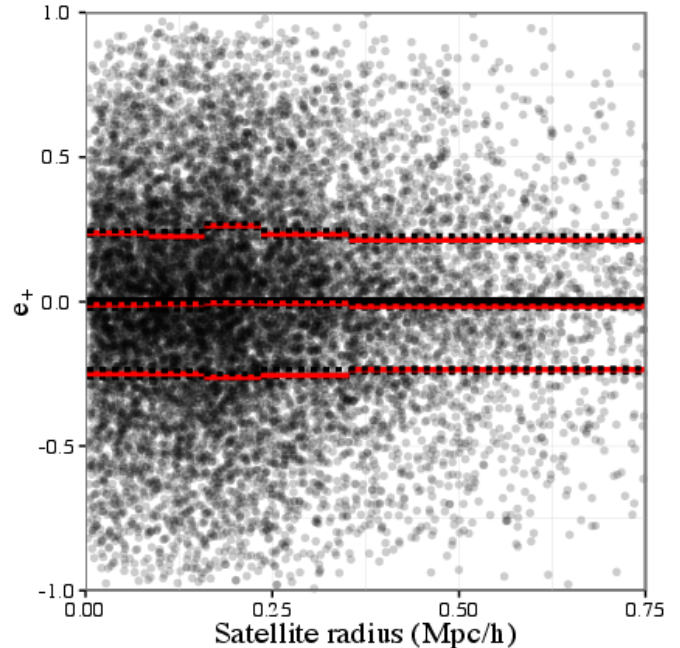


Figure 4. Ellipticity component measuring radial alignment derived from the REGLENS shapes for all groups with three or more members versus the projected physical distance from the group centre. There is no discernable dependence of the distribution of ellipticity components on physical radius. The red lines show quartiles of the distribution of e_+ components in radius bins. The black dashed lines show the error on the quartile measurements in each bin due to the finite number of galaxies.

plane of the sky, the mean ellipticity components e_+ and e_\times should both be consistent with zero while the mean position angle should be consistent with 45° . On the other hand, for perfect radial alignments (i.e. $\phi = 0$ for every galaxy in our catalogue) we would expect the mean e_+ to be equal to the mean ellipticity of our catalogue, $\langle e_+ \rangle \approx -0.46$, using the REGLENS shapes, and $\langle e_\times \rangle \approx 0$. Note that Fig. 4 is not intended as an assessment of the detection or non-detection of radial alignments. Rather, we conclude from the symmetric distribution in Fig. 4 that measurements of mean radial alignment statistics should yield informative and useful summaries of the properties of the full statistical distribution.

As described in Section 3.2, we created 25 mock catalogue realizations for each of our nine mocks at each point in a grid of μ and κ von Mises distribution parameter values. We then evaluated the posterior probability of the μ and κ values at each grid point given the measured mean alignment statistics. The 68%, 95% and 99% (‘‘1-3 sigma’’) posterior contours on μ and κ are shown in Fig. 5 for group multiplicity cuts of 3 and 21. The dashed lines show the posterior contours given the mean ellipticity components e_+ and e_\times while the dotted lines show the contours for the mean position angle. Because we consider only the mean ellipticity components or position angles, which are not sufficient statistics for describing the full distribution of position angles in our catalogue, we can gain additional information by combining the mean ellipticity components and position angles using a covariance matrix derived from the ensemble of mock catalogue realizations. For individual satellite galaxies e_+ and

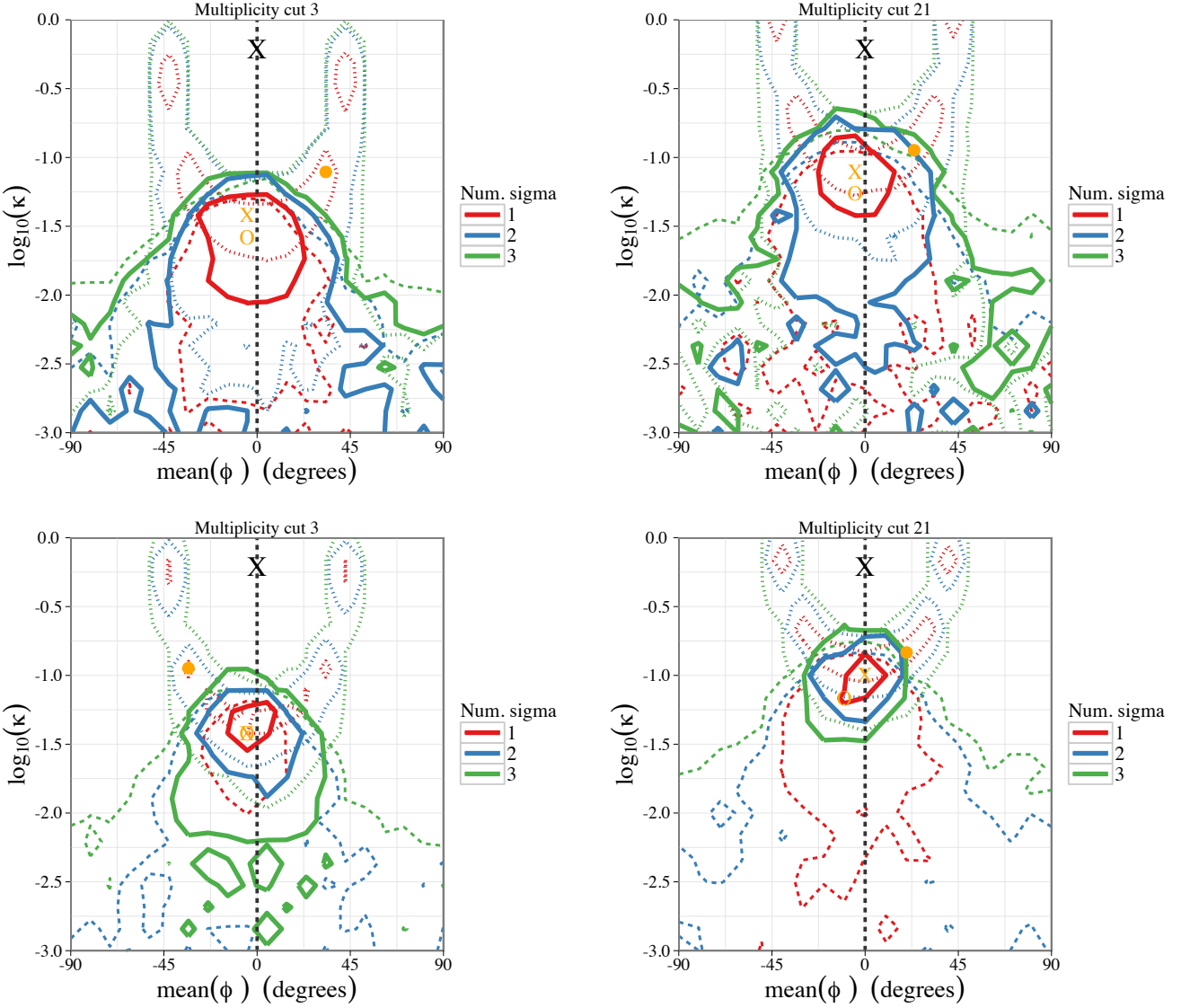


Figure 5. Con tours of the posterior probability distribution for the two parameters, $\mu = \langle 2\phi \rangle$ and κ , of the von Mises distribution for 2ϕ used to assign projected galaxy alignments in the mocks. The posterior is calculated given the combination of the mean ellipticity components and the mean position angles for group multiplicity cuts of 3 (left-hand panel) and 21 (right-hand panel). The top panels use the REGLens galaxy shape estimates while the bottom panels use the SIGMA shape estimates. The line styles denote posteriors for: mean ellipticity components (e_+ , e_x , dotted), mean position angle mapped to $[0, \pi/2]$ (dashed), and the combination of both statistics including the cross-covariance (solid). Although the ellipticity components and position angles are perfectly correlated for a single galaxy, the ensemble means of these quantities include some independent information allowing us to obtain tighter constraints with the combination of statistics. The orange open circle, filled circle, and “X” show the location of the maxima for each of these posteriors respectively. The black “X” near the top of each panel shows the model parameters for the cluster simulations shown by the short dashed green line in the right-hand panel of Fig. 1.

ϕ are perfectly correlated, but for our ensemble of mocks we typically find $\langle e_+ \rangle$ and $\langle \phi \rangle$ have a correlation coefficient ~ 0.85 . That is, the mean position angle cannot be derived from only the mean values of the ellipticity components and therefore contains some non-redundant information that can help further constrain the model for the alignment angle distribution. The solid lines in Fig. 5 show the posterior con tours when the mean ellipticity components and position angle are jointly used to constrain the von Mises distribution parameters. The top panels use radial alignment statistics

derived from the REGLens galaxy shape estimates while the bottom panels use SIGMA-derived galaxy shapes.

The closed dashed and dotted red con tours in the top panels in Fig. 5 show that the radial alignment signal is significant at no more than $\sim 1\text{-}\sigma$ using the REGLens galaxy shapes with either the ellipticity components or the position angle radial alignment estimators. Combining the two estimators, groups with 21 or more members show a radial alignment signal at $\sim 2\text{-}\sigma$ in the top right-hand panel of Fig. 5. The significance of the radial alignment detection increases to greater than $3\text{-}\sigma$ when using SIGMA to determine

the galaxy shapes as shown in the bottom panels of Fig. 5. The black “X” near the top of each panel denotes parameter values that reproduce the simulated alignments in Fig. 10 of Pereira et al. (2008). We rule out this model at more than $4\text{-}\sigma$ with either of our galaxy shape estimators under the assumption that projected galaxy shapes perfectly trace the projected shapes of dark matter haloes in the simulations of Pereira et al. (2008). The right-hand panel of Fig. 1 compares the best-fitting von Mises probability distributions for ϕ in Pereira et al. (2008) (short-dashed green line) and from our data using groups with three or more members and the REGLENS shapes (solid red line), corresponding to the orange cross in the top left-hand panel of Fig. 5.

In Fig. 6 we show the mean alignment statistics for different group multiplicity cuts. For a given multiplicity cut, we determine confidence intervals on the radial alignment measures by first maximizing the posterior for the von Mises distribution parameters μ and κ and then finding the 68% confidence intervals from the 25×9 mock realizations with specified μ and κ . We therefore quantify the uncertainty on the measured mean ellipticities and position angles using the width of the likelihood with fixed model parameters. This procedure is distinct from marginalizing the posterior for the von Mises distribution parameters, which would yield larger uncertainty intervals such that all our measurements would be consistent with a null signal. Because our model for the projected radial alignment angles in the mocks is merely descriptive, rather than physically motivated, we believe our method of uncertainty quantification suffices for the current analysis.

Our confidence intervals on the observed radial alignment measures are shown by the boxes in Fig. 6. The mean values from the mocks are shown by the horizontal lines in each box in Fig. 6. The circles and solid lines in Fig. 6 show the results using the REGLENS shape estimates while the triangles and dashed lines show those for the SIGMA shape estimates. Note that the circles and triangles in Fig. 6 show observed mean values while the lines in the centres of the boxes show predicted median values from the mocks. We include the mock-derived covariance between the mean ellipticity components and mean position angles when calculating the von Mises distribution parameters that maximize the posterior. Fig. 6 is one way to compare the effects of the group multiplicity cut and the choice of galaxy shape measure on the significance of the radial alignment detection, where we always choose the mock catalogue parameters that give the “best fit” to the observations (by maximizing the posterior). For a given galaxy shape estimator, the mean alignment measures in Fig. 6 are consistent for different multiplicity cuts, with the exception of those groups with 21 or more members, which show slightly stronger radial alignments at $1\text{-}\sigma$ significance.

We see in Fig. 6 that the SIGMA shapes yield mean radial alignment measures systematically further from the null values than the REGLENS shapes. As described in, e.g., Siverd et al. (2009) and Hung & Ebeling (2012), the position angle is potentially sensitive to systematic errors from poor angular resolution and close neighbours in the imaging. While corrections are made in Kelvin et al. (2012) for such systematic errors, we expect especially the SIGMA shapes to remain contaminated at some level by close neighbours. Because the number density of satellite galaxies increases

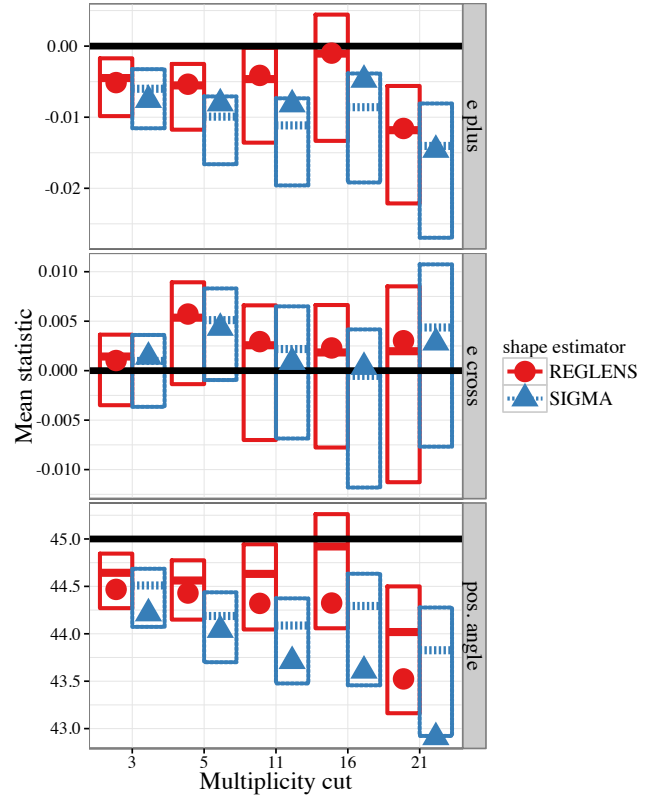


Figure 6. Mean ellipticity components and position angles in degrees as functions of the minimum group multiplicity. The points show the mean observed values while the box ranges show the 68% confidence intervals of the likelihoods given position angle distribution parameters chosen to maximize the conditional posterior given the observed mean ellipticities.

with decreasing projected group radius, it is possible that light bleeding from neighbouring galaxies could systematically affect the observed e_+ ellipticity component and position angle. Light bleeding from the BCG will introduce a systematic bias as well increasing the detected radial alignment. On the other hand, it is also possible that the outer shapes of galaxies as measured by SIGMA are more responsive to external tidal forces than the inner core of the galaxy. We therefore continue to present the results from our two shape estimators together to assist later interpretation of these effects.

In Fig. 6 we always maximize the (μ, κ) posterior given only the mean ellipticity components (i.e. neglecting the measured mean radial alignment angles), which is denoted by the orange filled circle in each panel of Fig. 5. We found it difficult to find mock radial alignment parameters that simultaneously provide good fits to both the mean ellipticity components and the mean position angles for the multiplicity cuts of 16 and 21 in Fig. 6. This could indicate that our mock radial alignment model is not sufficiently flexible to fit the data (i.e. more parameters are needed) or that there are numerous spurious position angle or ellipticity measurements in the high multiplicity groups. This model fitting choice is the reason that the points in the bottom panel of Fig. 6 are so far from the mock simulation mean values.

To look for potential group mass, radius, or redshift de-

pendence in the radial alignment signal, we recompute the mean radial alignment estimators in bins in the normalized group radius (r_p/r_{vir}) in Fig. 7, in group halo mass proxy (as described in Robotham et al. 2011) in Fig. 8, and in median group redshift in Fig. 9. Because galaxies with different morphologies could be expected to respond to tidal torquing in different ways, we also split our galaxy sample in Figs. 7, 8, and 9 according to the galaxy Sérsic indices measured in Kelvin et al. (2012). We define galaxies with a Sérsic index greater than 2 to be early-type and those with an index less than 2 to be late-type. This assigns 48% of our galaxy sample as early-type and 52% late-type.

The shaded boxes in Figs. 7, 8, and 9 again show the 68% confidence intervals on the mean radial alignment statistics derived from the mock realizations evaluated at the maximum posterior values for μ and κ , with the posterior maximized independently for each bin (rather than maximizing the joint posterior for all bin values simultaneously). Maximizing the posterior independently for each radius, mass, or redshift bin allows us to consider radial, mass, and redshift dependencies that are not explicitly modelled in the mocks. That is, rather than defining a radial, mass, and/or redshift dependence for μ and κ when generating mock realizations, we generate mocks with constant μ and κ values and then cut the mocks in the same way as the observed catalogue to quantify the radial alignment significance in each cut sub-sample independently. However, we cannot infer the joint significance of any radial, mass, or redshift dependence with our approach. Our measurements can identify important features needed in a radius-dependent model for the radial alignment angle distribution, but we are statistically limited by the size of our sample in constraining such a model.

Our radial alignment measures deviate from the expectation for random alignments at $1\text{-}\sigma$ significance in two of the three lowest radius bins for both shape estimators and galaxy types in Fig. 7. For the early-type galaxies, the largest radius bins in Fig. 7 show radial alignment measures that are consistent with tangential alignment at 99% confidence (or $3\text{-}\sigma$). But, we are statistically limited in drawing any conclusions from the measured values at large radii.

The tidal torquing mechanism predicts stronger radial alignments at smaller fractions of the virial radius (except at radii where satellite galaxies are at the perihelion of elliptical orbits, Pereira et al. 2008). Our uncertainties in Fig. 7 are too large to detect a radius dependence in the position angle distributions. We note again however, that our observed radial alignments are much weaker than that found for the alignments of haloes in N -body simulations (Knebe et al. 2008b). Our observed mean position angles are consistent at $2\text{-}\sigma$ with previous measurements using SDSS isophotal shapes (Pereira & Kuhn 2005; Faltenbacher et al. 2007), which found equivalent values of $\langle\phi\rangle \sim 42\text{--}44^\circ$ with $\langle\phi\rangle$ increasing with increasing group radius. However we systematically favour mean position angles closer to 45° than in previous SDSS isophotal measurements, which we attribute to the PSF correction in our two shape estimators as discussed further in Appendix A. The mean e_x ellipticity component is always consistent with zero in agreement with our expectations in the absence of dominant systematic errors in the shape measurements.

Because all mass bins in Fig. 8 are consistent within

the uncertainties, we do not detect any host halo mass dependence in the radial alignment distributions. The highest group mass bin in Fig. 8 ($M > 10^{14} h^{-1} M_\odot$) has a non-null detection of radial alignments at 68% confidence for both galaxy types and shape estimators. It is noteworthy in this context that Knebe et al. (2008a,b) find that the sub-halo radial alignment distributions in N -body simulations are independent of host halo mass.

Similarly in Fig. 9 we do not detect any redshift dependence in the radial alignment distributions, except for early-type galaxies using the SIGMA-derived shapes. In that case, the lowest and highest redshift bins are inconsistent within their 68% confidence intervals, with the radial alignments stronger at high redshift. The significant radial alignment in the two highest redshift bins for early-type galaxies in Fig. 9 (versus null detections in the two lowest redshift bins) may be due to a correlation between halo mass proxy and redshift in our catalogue. Within the highest mass bin in Fig. 8, 40% of the groups have redshifts greater than 0.25 and are therefore also in the highest redshift bin in Fig. 9. But, our catalogue is too small to explore this correlation in more detail.

4.1 Lensing contamination

Our measurement of $\langle e_+ \rangle$ can be used to estimate the contamination of the weak lensing signal around galaxy groups when galaxies in the lens plane are confused with background source galaxies due to photometric redshift uncertainties.

The surface mass density contrast is often measured to estimate masses of isolated objects from weak lensing (e.g. Blazek et al. 2012),

$$\Delta\Sigma = \Sigma_c \left(\gamma_+^G + \gamma_+^{\text{IA}} \right), \quad (6)$$

where γ_+^G is the tangential galaxy shear induced by lensing, γ_+^{IA} is a spurious shear due to intrinsic alignments of lens-plane galaxies that are mixed with the source sample, and Σ_c is the lensing critical surface mass density (e.g. Bartelmann & Schneider 2001).

The shear is related to the observed ellipticity by the shear responsivity, $\gamma \approx \langle e \rangle / 2\mathcal{R}$. The amount of intrinsic alignment contamination also depends on the fraction of “source” galaxies that are actually at the redshift of the lens plane (Fischer et al. 2000). This depends on the photometric redshift uncertainty and the projected radius from the centre of the group as the number density of lens-plane galaxies increases towards the group centre. The dependence of the source sample contamination on group radius is called the “boost factor” $B(r)$ in Blazek et al. (2012), where $(B(r) - 1)/B(r)$ is the fraction of lens-plane galaxies in the source sample.

Assuming $\mathcal{R} = 0.87$, our observed e_+ for groups with three or more members implies

$$\Delta\Sigma = -10 \pm 200 \times (B(r) - 1) \quad h M_\odot \text{pc}^{-2}, \quad (7)$$

at a mean radius of the sample of $\sim 300 h^{-1} \text{kpc}$, and where the errors are dominated by the sample variance estimated from the mock group catalogues and give the $1\text{-}\sigma$ uncertainties. For haloes of massive early type galaxies and an assumed photometric redshift contamination at this radius of

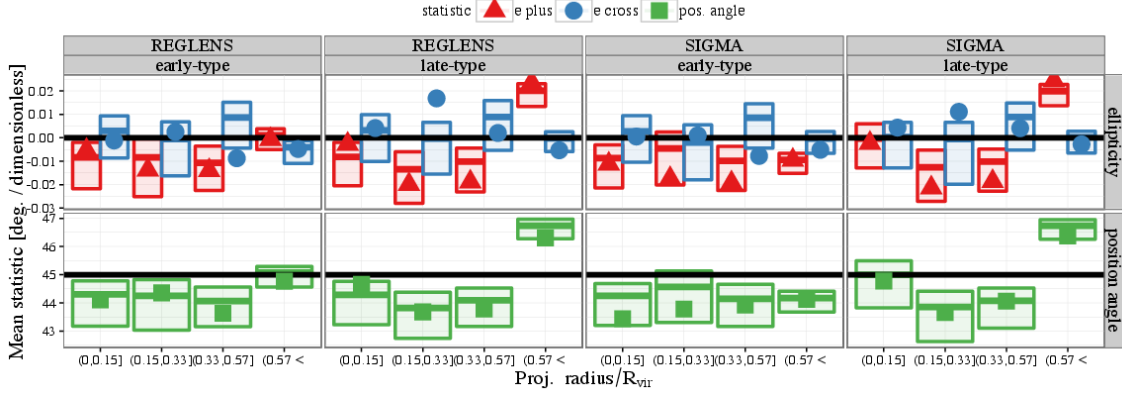


Figure 7. Mean ellipticity components and position angles similar to Fig. 6 but with multiplicity cut fixed at 3 and binned in normalized projected group radius. In contrast to Fig. 6, the confidence intervals are chosen by maximizing the joint posterior for the position angle distribution parameters given both the observed mean ellipticity components and mean position angles, with each bin considered separately.

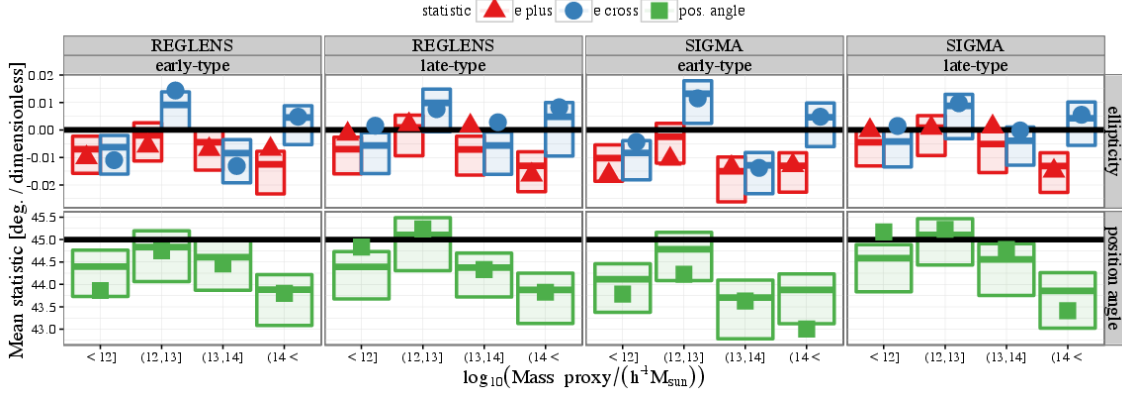


Figure 8. Mean ellipticity components and position angles similar to Fig. 7 but binned in the logarithm of the group mass proxy. The mass proxies are derived by matching the observed group sizes and velocity dispersions to those in the GAMA mock catalogues and taking matched dark matter halo masses (Robotham et al. 2011), where the halo masses are those of the GALFORM Dhaloes (Helly et al. 2003) that are roughly equivalent to the enclosed mass equal to 200 times the critical density.

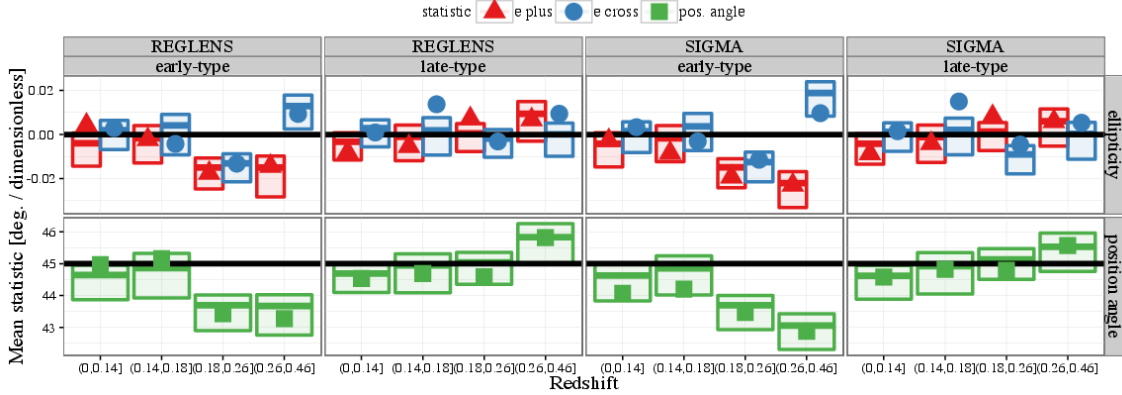


Figure 9. Mean ellipticity components and position angles similar to Fig. 7 binned in the median group redshift.

$B(r) - 1 = 0.1$, the estimated $\Delta\Sigma$ in equation (7) is approximately $-1 \pm 20\%$ of the lensing signal measured in Mandelbaum et al. (2006b).

5 CONCLUSIONS

We have constrained the distribution of satellite galaxy radial alignment angles within GAMA groups independently as functions of group multiplicity, radius, mass proxy, and redshift. For all subsets of our catalogue and definitions of galaxy shape estimators we consider, we observe a statistically weak radial alignment signal that is different from the predictions from dark matter N -body simulations. Our comparisons with simulations are complicated by the fact that most published simulations make predictions about (unobservable) dark matter alignments, rather than observable baryon alignments. We conclude that our measurements give strong evidence for large misalignments between dark matter and baryonic (i.e. stellar) shapes, which imply there are fundamental and important baryonic physical processes that decouple the baryons from the dark matter in group and cluster environments (e.g. Sharma et al. 2012). However, it is also possible that the dark matter may still be coupled with the baryons and have the same alignments, in which case the predictions of the dark matter alignments from simulations are incorrect. We consider this latter possibility unlikely, but mention it here for completeness.

The degree and significance of the radial alignment statistics depend on the method used to measure satellite galaxy shapes. Using PSF-corrected 2D model fits measured in SDSS imaging to define satellite galaxy orientations (Kelvin et al. 2012), we detect satellite radial alignments at greater than 99% confidence for all group multiplicities, but with mean position angles systematically larger than previous measurements in SDSS (that had no PSF corrections). Using galaxy shape estimates optimized for weak lensing, we detect radial alignments at a weaker 95% confidence but find best-fitting radial alignment angle distributions of similar width to those inferred from the SIGMA shapes. We use an ensemble of mock group catalogues based on N -body simulations to estimate the sample variance errors of our measurement, which are the dominant source of uncertainty.

For both our galaxy shape estimators, our non-uniform radial alignment detections are most significant at group radii less than $\sim 0.4 r_{\text{vir}}$, at group masses larger than $\sim 10^{14} h^{-1} M_{\odot}$, or at redshifts larger than ~ 0.17 . But we do not have sufficient statistics to bin in combinations of these group properties. Also, our sample variance-dominated uncertainties are too large to detect any clear dependence of the radial alignments on group radius, mass or redshift. Finally we note that radial alignment measurements at small radii and high redshifts are most likely to be susceptible to systematics such as position angles errors at small radius and less accurate galaxy sizes and ellipticity measurements for small galaxies at high redshift.

While the trends in our data are consistent with the predictions from N -body simulations that find radial alignments to be created by tidal torquing within the group gravitational potential, our measured alignments using either of our galaxy shape estimators are weaker than any existing

predictions in the literature. We speculated that the slightly larger radial alignments detected using the galaxy Sérsic model fits may indicate that tidal torquing acts to align the outer shapes of galaxies more efficiently, but we are limited in exploring this mechanism further by our sample size.

The radial alignments of satellite galaxies are also a concern for weak lensing measurements of group and cluster masses when lens and source galaxy samples must be inferred via photometric redshifts (e.g. Blazek et al. 2012). If the galaxies in the lens plane have strong intrinsic alignments and if some lens plane galaxies are mistaken for background sources, the lensing measurements can become biased. With our observed mean ellipticity components that include typical lensing inverse noise weights, we have discovered that intrinsic alignments may be less than a 20% contamination for photometric weak lensing measurements of high mass groups. We leave a more thorough modelling of the intrinsic alignment contamination in lensing measurements for further work. Our results also have implications for the magnitude of the small-scale intrinsic galaxy alignment contamination to cosmic shear measurements, where the predictions of Schneider & Bridle (2010) are likely to be an overestimate of the small-scale cosmic shear contamination.

In future work we also plan to study the 3D shapes of sub-haloes in the GAMA mocks to understand both what 3D misalignments are required to match the observations and how the projection of 3D triaxial galaxy shapes should be interpreted (see, e.g. Bett 2012).

ACKNOWLEDGEMENTS

We thank Jonathan Blazek for helpful feedback on an early version of this paper and an anonymous referee for many helpful improvements including the suggestion to measure alignments for different galaxy morphologies. PN acknowledges a Royal Society URF and ERC StG grant (DEGAS-259586). Part of this work performed under the auspices of the U.S. Department of Energy by Lawrence Livermore National Laboratory under Contract DE-AC52-07NA27344.

GAMA is a joint European-Australasian project based around a spectroscopic campaign using the Anglo-Australian Telescope. The GAMA input catalogue is based on data taken from the Sloan Digital Sky Survey and the UKIRT Infrared Deep Sky Survey. Complementary imaging of the GAMA regions is being obtained by a number of independent survey programs including *GALEX* MIS, VST KIDS, VISTA VIKING, *WISE*, Herschel-ATLAS, GMRT and ASKAP providing UV to radio coverage. GAMA is funded by the STFC (UK), the ARC (Australia), the AAO, and the participating institutions. The GAMA website is <http://www.gama-survey.org/>.

Funding for the SDSS and SDSS-II has been provided by the Alfred P. Sloan Foundation, the Participating Institutions, the National Science Foundation, the U.S. Department of Energy, the National Aeronautics and Space Administration, the Japanese Monbukagakusho, the Max Planck Society, and the Higher Education Funding Council for England. The SDSS Web Site is <http://www.sdss.org/>. The SDSS is managed by the Astrophysical Research Consortium for the Participating Institutions. The Participat-

ing Institutions are the American Museum of Natural History, Astrophysical Institute Potsdam, University of Basel, University of Cambridge, Case Western Reserve University, University of Chicago, Drexel University, Fermilab, the Institute for Advanced Study, the Japan Participation Group, Johns Hopkins University, the Joint Institute for Nuclear Astrophysics, the Kavli Institute for Particle Astrophysics and Cosmology, the Korean Scientist Group, the Chinese Academy of Sciences (LAMOST), Los Alamos National Laboratory, the Max-Planck-Institute for Astronomy (MPIA), the Max-Planck-Institute for Astrophysics (MPA), New Mexico State University, Ohio State University, University of Pittsburgh, University of Portsmouth, Princeton University, the United States Naval Observatory, and the University of Washington.

REFERENCES

- Adami C., Gavazzi R., Cuillandre J. C., Durret F., Ilbert O., Mazure A., Pelló R., Ulmer M. P., 2009, *A&A*, 493, 399
- Agustsson I., Brainerd T. G., 2006, *ApJ*, 644, L25
- Baldry I. K. et al., 2010, *MNRAS*, 404, 86
- Bartelmann M., Schneider P., 2001, *Phys. Rep.*, 340, 291
- Bernstein G. M., Norberg P., 2002, *AJ*, 124, 733
- Bett P., 2012, *MNRAS*, 420, 3303
- Blazek J., Mandelbaum R., Seljak U., Nakajima R., 2012, *ArXiv e-prints*
- Dekel A., 1985, *ApJ*, 298, 461
- Djorgovski S., 1983, *ApJ*, 274, L7
- Driver S. P. et al., 2011, *MNRAS*, 413, 971
- Driver S. P. et al., 2009, *Astronomy and Geophysics*, 50, 050000
- Faltenbacher A., Li C., Mao S., van den Bosch F. C., Yang X., Jing Y. P., Pasquali A., Mo H. J., 2007, *ApJ*, 662, L71
- Fischer P. et al., 2000, *AJ*, 120, 1198
- Hao J., Kubo J. M., Feldmann R., Annis J., Johnston D. E., Lin H., McKay T. A., 2011, *ApJ*, 740, 39
- Hawley D. L., Peebles P. J. E., 1975, *AJ*, 80, 477
- Helly J. C., Cole S., Frenk C. S., Baugh C. M., Benson A., Lacey C., 2003, *MNRAS*, 338, 903
- Hill D. T. et al., 2011, *MNRAS*, 412, 765
- Hirata C., Seljak U., 2003, *MNRAS*, 343, 459
- Hirata C. M. et al., 2004, *MNRAS*, 353, 529
- Hui L., Zhang J., 2008, *ApJ*, 688, 742
- Hung C.-L., Ebeling H., 2012, *MNRAS*, 2495
- Kelvin L. S. et al., 2012, *MNRAS*, 421, 1007
- Kirk D., Bridle S., Schneider M., 2010, *MNRAS*, 408, 1502
- Knebe A., Draganova N., Power C., Yepes G., Hoffman Y., Gottlöber S., Gibson B. K., 2008a, *MNRAS*, 386, L52
- Knebe A., Libeskind N. I., Knollmann S. R., Yepes G., Gottlöber S., Hoffman Y., 2010, *MNRAS*, 405, 1119
- Knebe A., Yahagi H., Kase H., Lewis G., Gibson B. K., 2008b, *MNRAS*, 388, L34
- Kuhlen M., Diemand J., Madau P., 2007, *ApJ*, 671, 1135
- Lund U., Agostinelli C., 2009, *CircStats: Circular Statistics*, from "Topics in Circular Statistics" (2001). R package version 0.2-4
- Mandelbaum R., Hirata C. M., Ishak M., Seljak U., Brinkmann J., 2006a, *MNRAS*, 367, 611
- Mandelbaum R. et al., 2005, *MNRAS*, 361, 1287
- Mandelbaum R., Seljak U., Kauffmann G., Hirata C. M., Brinkmann J., 2006b, *MNRAS*, 368, 715
- Pereira M. J., Bryan G. L., 2010, *ApJ*, 721, 939
- Pereira M. J., Bryan G. L., Gill S. P. D., 2008, *ApJ*, 672, 825
- Pereira M. J., Kuhn J. R., 2005, *ApJ*, 627, L21
- Plionis M., Benoist C., Maurogordato S., Ferrari C., Basilakos S., 2003, *ApJ*, 594, 144
- Robotham A. et al., 2010, *PASA*, 27, 76
- Robotham A. S. G. et al., 2011, *MNRAS*, 416, 2640
- Schneider M. D., Bridle S., 2010, *MNRAS*, 402, 2127
- Sharma S., Steinmetz M., Bland-Hawthorn J., 2012, *ApJ*, 750, 107
- Sivard R. J., Ryden B. S., Gaudi B. S., 2009, *arXiv:0903.2264*
- Song H., Lee J., 2012, *ApJ*, 748, 98
- Thakar A., Szalay A., Fekete G., Gray J., 2008, *Computing in Science Engineering*, 10, 30
- Wesson P. S., 1984, *A&A*, 138, 253

APPENDIX A: GALAXY ISOPHOTAL SHAPE COMPARISON

In Section 2.2 we introduced two methods for estimating galaxy shapes, the REGLens pipeline optimized for weak lensing measurements and *r*-band Sérsic model fits (SIGMA). For the Sérsic fits, we use the output of the SIGMA pipeline developed for the GAMA survey and described in Kelvin et al. (2012). However many previous measurements of galaxy radial alignments in the literature have relied on isophote measurements provided in the SDSS CAS catalogue. For the measurements we present here, a key difference between the SIGMA and CAS pipelines is that SIGMA includes corrections for the rounding effect of the PSF that are not applied in the CAS measurement. We also note that the CAS catalogue does not provide any isophote measurement uncertainties. In this section we compare some galaxy properties derived from the SDSS CAS and GAMA SIGMA pipelines. For completeness, we also include results from the GAMA team IOTA pipeline that is based on non-PSF corrected nine-band isophote measurements (Hill et al. 2011, Liske, in preparation). Because of the lack of PSF correction, we expect the IOTA and CAS measurements to be similar in yielding rounder galaxy shapes than the SIGMA and REGLens pipelines.

In the left-hand panel of Fig. A1 we show the galaxy ellipticity magnitudes derived from both the CAS and IOTA isophote measurement pipelines compared with the SIGMA measurements. As expected, the SIGMA ellipticities are systematically larger than those derived from the CAS and IOTA catalogues with a nonlinear relationship between the bias and the ellipticity magnitude (round galaxies stay round after PSF convolution).

We compare the radial projected position angles (as defined in the left-hand panel of Fig. 1) in the right-hand panel of Fig. A1. There is much larger scatter between the position angle measurements than in Fig. 3, including 25% of all galaxies with position angle mismatches larger than 15°. Restricting the comparison to galaxies with major axes spanning more than 12 SDSS pixels and ellipticity magnitude

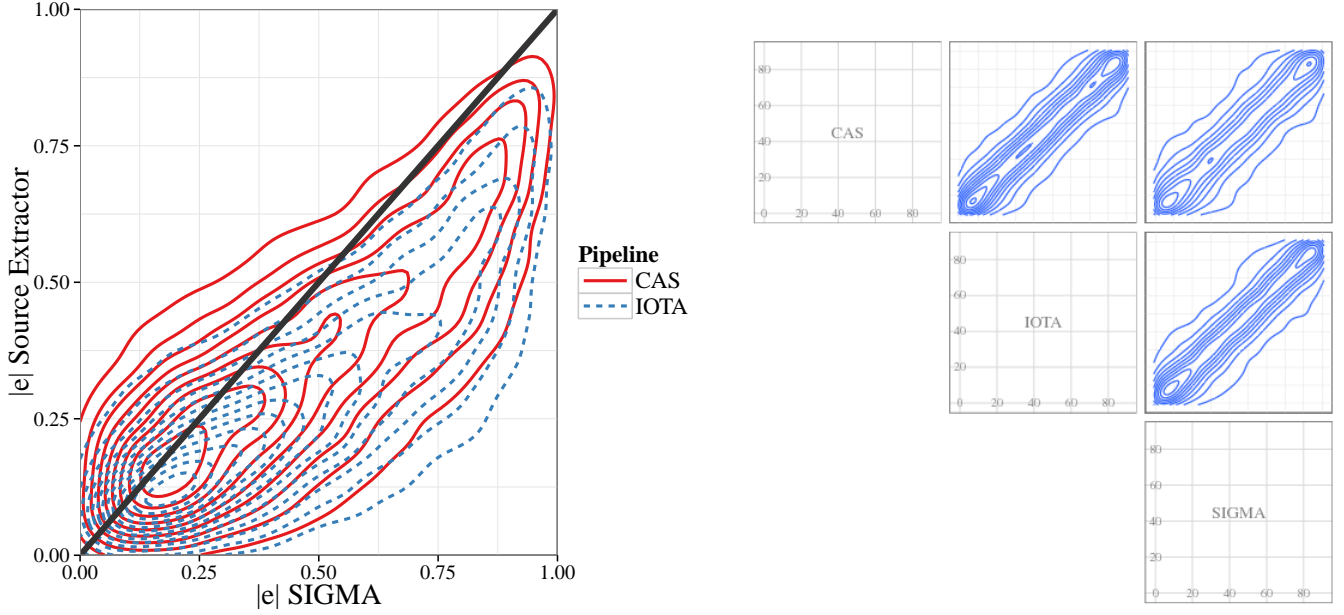


Figure A1. Comparison of galaxy shape properties using the SDSS CAS (isophotal) and GAMA SIGMA (model fit) and IOTA (isophotal) measurements (based on similar SDSS imaging data). The left-hand panel compares the ellipticity magnitudes while the right-hand panel compares the radial position angles with respect to the group centres.

greater than 0.2 reduces the fraction of galaxies with position angle mismatches larger than 15° to 15%. This trend is qualitatively consistent with the expectation that the PSF would mostly affect the observed orientations of rounder galaxies with smaller angular sizes.

In Fig. A2 we plot the mean radial alignment statistics as functions of minimum group multiplicity as in Fig. 6. The error bars here show solely the measurement uncertainties, while the much larger sample variance errors are omitted. For both the e_+ and position angle statistics, the isophotal shapes from the CAS catalogue yield systematically stronger radial alignment measurements than those from the SIGMA pipeline. The mean position angles measured with the CAS and IOTA catalogues show a less consistent trend however. The e_x component in the middle panel of Fig. A2 (which is expected to be zero in the absence of systematics) has comparable magnitude for both isophote measurement pipelines. We therefore conclude that the uncorrected effects of the PSF in the SDSS CAS catalogue isophote measurements are likely to cause overestimates of the radial alignment of galaxies in groups and clusters. This is an important effect to consider when comparing our results with previous measurements relying on the SDSS catalogue.

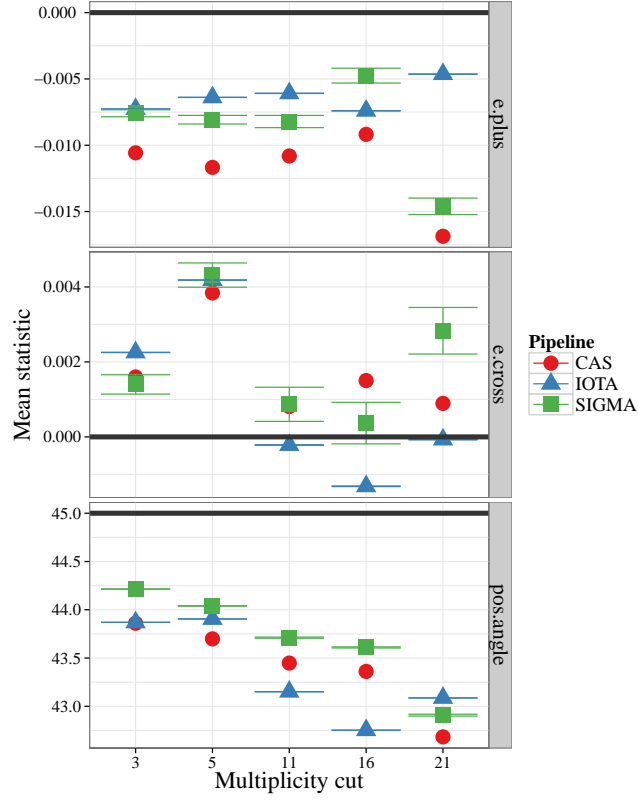


Figure A2. Mean radial alignment statistics with different minimum group multiplicity cuts. The circles show the mean statistics derived when using the 25 mag per square arcsec. isophotes from the SDSS DR7 **CAS** catalogue to estimate galaxy shapes and orientations. The triangles show analogous results when the galaxy isophotes are derived from the same SDSS imaging data but using the **IOTA** pipeline developed for the GAMA survey (Kelvin et al. 2012). The error bars for the **IOTA** measurements show the error on the mean statistics derived by formally propagating the measurement errors on the isophote axis measurements for each galaxy. There are no such error estimates supplied in the **CAS** catalogue. The squares show the **SIGMA** derived values (based on Sérsic model fits), which are those used in the main body of the paper.